IEEE Access
Multidisciplinary | Rapid Review | Open Access Journal

Received May 8, 2019, accepted May 28, 2019, date of publication June 26, 2019, date of current version July 18, 2019.

Digital Object Identifier 10.1109/ACCESS.2019.2925051

MRI Reconstruction From Sparse K-Space Data Using Low Dimensional Manifold Model

SAIM ABDULLAH[1], OMAR ARIF[1], (Member, IEEE), M. BILAL ARIF[2], AND TAHIR MAHMOOD[3]
[1]School of Electrical Engineering and Computer Science, National University of Sciences and Technology (NUST), Islamabad 44000, Pakistan
[2]Department of General Medicine, CMH Pano Aqil, Pano Aqil 65120, Pakistan
[3]Benazir Bhutto Shaheed Teaching Hospital (DHQ), Abbottabad, Pakistan

Corresponding author: Omar Arif (omar.arif@seecs.edu.pk)

ABSTRACT Recent compressed sensing (CS) approaches to utilize the similarity and redundancy of magnetic resonance (MR) image patches to enable reconstruction from sparse k-space measurements. In this paper, the patches' similarity and redundancy are exploited by applying the low-dimensional manifold model (LDMM). The basic assumption of the LDMM is that the image patches sample a manifold whose intrinsic dimensions are much lower than the high-dimensional ambient space. MR images also exhibit a low-dimensional patch-manifold structure. Based on this assumption, the dimension of the patch-manifold is used as a regularizer in a variational formulation. The MR image is then reconstructed by keeping the dimension of the patch manifold as small as possible. The proposed algorithm significantly increases the quality of the reconstructed images. The algorithm is evaluated on two datasets containing 100 MR images each. The reconstruction quality of the algorithm, gauged using three quality metrics: peak signal-to-noise ratio, structural similarity index measure, and normalized root-mean-square error, is better than the comparison methods.

INDEX TERMS MRI reconstruction, sparse recovery, compressed sensing, manifold learning.

I. INTRODUCTION

Magnetic resonance imaging (MRI) enables the visualization of anatomical structures and the physiological processes of the internal body. It is a noninvasive imaging technique and is widely used in medical diagnosis and research. However, the acquisition speed of MRI is slow as the MRI data is obtained by sequentially traversing curves in the multidimensional k-space. In spite of the advances in hardware, the traversal speed is constraint by a combination of physical and physiological conditions [1]. Various approaches have been used to accelerate the MRI acquisition process. Parallel imaging (PI) [2] is a hardware-based approach that combines the signals received from several receiver coils with different sensitivities to reconstruct the images. Another approach is to apply the compressed sensing (CS) [3] theory to MRI reconstruction [4], [5]. The basic idea of CS-MRI is to reconstruct MR images from significantly fewer measurements by utilizing the sparsity of MR images in an appropriate transform domain. Three requirements must be fulfilled for successful CS application [5]: transform sparsity, incoherent under-sampling, and a nonlinear reconstruction method. Conventional CS-MRI reconstruction methods use universal sparsifying transforms, such as Total Variation (TV), Fourier transform and wavelet transform [4], [6], [7]. Total variation regularization exploits the sparsity of the gradients and is often included in the objective function even when other sparsifying transforms are present [4]. CS-MRI has also been applied to dynamic MRI [8]–[12], which are sparse in both the space and time domain. The main disadvantage of applying universal global transforms is that they are not specific to the image and the reconstruction may suffer when the data is highly under-sampled because of insufficient sparse representation [13]. This has led to the use of patch-based sparsifying methods that can generate data specific dictionaries, which can better capture the local image features and thereby favoring better sparsities at much higher under-sampling rates [13]–[17]. In [17], convolutional sparse coding is successfully applied for MRI reconstruction. Patch-based non-local methods have also been used to sparsify the MR images by using the similarity and redundancy of Non- local patches [18]–[23]. Non-local methods have been shown to preserve the image quality better than the conventional CS construction [20]. Deep learning-based

The associate editor coordinating the review of this manuscript and approving it for publication was Trivikram Rao Molugu.

methods have also been applied to MRI reconstruction such as [24], [25]. However, these methods require many training examples which may not be possible to obtain in all situations, especially in medical images.

Recently [26] proposed a patch-based low dimensional manifold model (LDMM) for image inpainting and denoising. The basic assumption of LDMM is that the image patches sample a manifold whose intrinsic dimensions are much lower than the high dimensional ambient space. Based on this assumption, the image is recovered by keeping the dimension of the patch-manifold as small as possible. Split Bregman iteration [27] is used to solve the optimization problem. The key step requires solving a Laplace-Beltrami equation, which is solved via the point integral method (PIM) [28], [29].

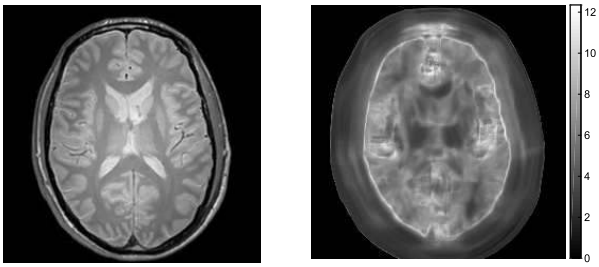

FIGURE 1. Patch manifold dimensions. [Left] an MR image. Patch-manifold is constructed from patches of size 16 × 16. [Right]: local dimension of the patch manifold color coded on the image. The local dimensions of the patch-manifold do not exceed 12, which shows that image has low dimensional structure while accommodating rich structural information.

LDMM has been applied to general image processing [26], scientific data interpolation [30] and hyperspectral image reconstruction [31], where it has achieved state-of-the-art results. MR images also exhibit low dimensional patch manifold structure. As an example, we extract patches of size 16×16 from an MR image shown in Figure 1. The patches form a point cloud, which sample a manifold embedded in R^{256}. The local dimension of the point cloud is computed using the technique described in [32]. The obtained piecewise dimensions are color coded on the image as shown in Figure 1. The dimension of the patch manifold does not exceed 12, which shows that image has low dimensional structure while accommodating rich structural information. Inspired by the low dimensional manifold model and non-local methods, we use LDMM regularization to reconstruct MR image from highly under-sampled k-space measurements. However, it should be noted that MR image formation process is fundamentally different as the MR data is partially available in k-space rather than in the image space. In the context of dynamic MRI reconstruction, manifold learning techniques [33] have been used before. However, these approaches apply manifold learning-based techniques to whole image and not to image patches and thus fail to utilize the similarity and redundancy of local patches of the MR images. For example, in [34], [35], manifold learning is used to generate the self-gating signal. Similarly, Chen *et al.* [36] employ locally linear embedding [37] to learn a multidimensional self-gating signal, which is then used to group the k-space profiles. The reconstruction is then performed using non-linear FFT on the grouped profiles. Podder and Jacob [35] use graph Laplacian-based regularization formulation to recover the dynamic MR images. The structure of the manifold is estimated using the samples acquired at the same sampling location for each frame.

In Section II, we briefly describe the LDMM approach followed by the proposed method in Section III. The results are given in Section IV. Section VI concludes the paper. This work expands upon the work presented in a conference.[1]

II. LOW DIMENSIONAL MANIFOLD MODEL

Recently, LDMM [26] was proposed for general image processing tasks such as subsampled image reconstruction and it showed promising results. For a given image s, let $P(s)$ be the collection of all patches of size $\sqrt{d} \times \sqrt{d}$ obtained from the image. $P(s)$ forms a point cloud in $\mathbb{R}^d$. The basic idea is that this point cloud samples a smooth low dimensional manifold embedding in $\mathbb{R}^d$. The dimensions of the patch manifold $\dim(\mathcal{M})$ can be used as a regularizer. The local dimensions of the manifold embedded in R^d are calculated using the following formula [26]

$$\dim(\mathcal{M}) = \sum_{j=1}^{d} \|\nabla_{\mathcal{M}} \alpha_j(x)\|^2 \tag{1}$$

where $\alpha = \{\alpha_i\}_{i=1}^{d}$ are the coordinate functions on $\mathcal{M}$, i.e. $\alpha_i(x) = x^i, \forall x = (x^1, \cdots, x^d) \in \mathcal{M}$. Given the above definition, the optimization problem for the recovery of image can be written as

$$\underset{s,\mathcal{M}}{\operatorname{argmin}} \sum_{j=1}^{d} \|\nabla_{\mathcal{M}} \alpha_j\|^2_{L^2(\mathcal{M})} + \|\Phi s - m\|^2, \tag{2}$$

$$\text{subject to } P(s) \subset \mathcal{M}, \tag{3}$$

where $\|\nabla_{\mathcal{M}} \alpha_j\|^2_{L^2(\mathcal{M})} = \int_{\mathcal{M}} \|\nabla_{\mathcal{M}} \alpha_j(x)\|^2 dx$ and Φ is the measurement operator that causes some damage to the image and m represents the acquired measurements.

The optimization (2) is solved using iterative method. The key part of the algorithm is to use point integral method (PIM) [28] to solve the Laplace-Beltrami equation on the patch point cloud, and it has shown much better results as compared to using graph Laplacian. The details are presented in the next section, where we explain the procedure with respect to MR image reconstruction.

III. PROPOSED METHODOLOGY

The under-sampled MRI data (k-space measurements) can be modeled as:

$$m = F_u s + \eta, \tag{4}$$

where $s \in \mathbb{R}^n$ is the MR image to be reconstructed, $m \in \mathbb{C}^m$ is the acquired k-space data and $F_u = UF$ is the under-sampled

[1] IEEE-EMBS International Conference on Biomedical and Health Informatics 2019

Fourier transform, where U is the $m \times n$ undersampling matrix. Inspired by the LDMM framework [26], we assume that the patches of the MR image s sample a smooth low dimensional manifold $\mathcal{M}$ embedded in a high dimensional space $\mathbb{R}^d$. Let $P(s)$ be a collection of all such patches, such that each pixel of the image s appears with same frequency in different patches. This overlapping strategy for the generation of patches will allow faster computations in the reconstruction algorithm [22] (See Equation (13)). $P(s)$ can be thought of as a matrix of size $d \times n$, where d and n are the patch and image sizes in pixels, respectively. Each column of the matrix $P(s)$ represent one patch and rows of the patch matrix can be seen as shifted version of the image. Using dimension of the patch manifold as regularizer, the optimization problem for the recovery of MR image can be written as:

$$\begin{aligned} &\underset{s,\mathcal{M}}{\operatorname{argmin}} \sum_{j=1}^{d} \|\nabla_{\mathcal{M}}\alpha_j\|^2_{L^2(\mathcal{M})} + \lambda\|F_u s - m\|^2, \qquad (5)\\ &\text{subject to } \; P(s) \subset \mathcal{M}, \end{aligned}$$

An iterative procedure is used to solve the above optimization problem. In each iteration, first we update the image and manifold coordinate functions α_i, while keeping the manifold fixed. Later, the manifold is updated. Update of $\mathcal{M}$ is straight forward ($\mathcal{M} = \{\alpha_1(x), \cdots, \alpha_d(x) : x \in \mathcal{M}\}$). The difficult part is to solve Equation (5) for image and coordinate functions for which split-Bregman iteration is used [27]:

$$\alpha^* = \arg\min_{\alpha} \sum_{j=1}^{d} \|\nabla_{\mathcal{M}}\alpha_j\|^2_{L^2(\mathcal{M})} + \mu\|\alpha(P(s)) - P(s) + Q\|^2 \qquad (6)$$

$$s^* = \arg\min_{s} \lambda\|F_u s - m\|^2 + \mu\|\alpha(P(s)) - P(s) + Q\|^2 \qquad (7)$$

$$Q^* = Q + \alpha(P(s)) - P(s)$$

where $\alpha(P(s)) = \begin{pmatrix} \alpha_1(P(s)) \\ \vdots \\ \alpha_d(P(s)) \end{pmatrix} \in \mathbb{R}^{d\times n}$ $\alpha_i(P(s)) = (\alpha_i(x))_{x\in P(s)}$, and μ is the penalty parameter.

The solution of Equation (6) by standard variational methods is given by the following Laplace-Beltrami equations over the manifold

$$\begin{cases} \Delta_{\mathcal{M}} u(x) + \mu \sum_{y\in P(s)} \delta(x-y)(u(x) - v(y)) = 0, & x \in \mathcal{M} \\ \dfrac{\partial(u)}{\partial \mathrm{n}}(x) = 0, & x \in \partial\mathcal{M}, \end{cases} \qquad (8)$$

where u is any one of the α_is, v is the given function on the manifold, $\partial(\mathcal{M})$ is the boundary of $\mathcal{M}$, and n is the outward normal.

If the manifold is represented by a mesh, the finite element method is quite effective in solving the above PDE. However, for a unstructured manifold, it is very difficult to solve (8). Usually, graph Laplacian operator is used to approximate the Laplace-Beltrami of the manifold. However, as pointed out in [26], graph Laplacian is an inconsistent method due to the lack of boundary correction. In [26], the authors solve the Laplace-Beltrami equation using the Point Integral Method (PIM) [28], [29]. The PIM approximates (8) with an integral equation which can be easily discretized. In PIM, the solution to Equation (8) can be well approximated by the solution of the following integral equation [26], [28]

$$\int_{\mathcal{M}} (u(x) - v(y))R_t(x,y)\mathrm{d}y + \mu t \sum_{y\in P(s)} R_t(x,y)u(y) - v(y) = 0 \qquad (9)$$

where $R_t(x,y) = C_t \exp(\frac{|x-y|^2}{4t})$. The integral equation can be discretized easily as:

$$\frac{|\mathcal{M}|}{n}\sum_{j=1}^{n} R_t(x_i,x_j)(u(x_i) - u(x_j)) + \mu t \sum_{j=1}^{n} R_t(x_i,x_j)u(x_j) - v(x_j) = 0 \qquad (10)$$

where $|\mathcal{M}|$ is the volume of $\mathcal{M}$.

Using matrix notation, Equation 10 can be written as:

$$(L + \mu W)u = \mu W v, \qquad (11)$$

where $u = (u(x_1), \cdots, u(x_n))^T$, v is the corresponding row if $(P(s) - Q)$ and W is a $n \times n$ weight matrix with entries $W_{ij} = R_t(x_i, x_j)$. D is a diagonal matrix with $d_i = \sum_{j=1}^{n} W_{ij}$ and $L = D - W$. The linear system in Equation (11) is asymmetric and is solved using generalized minimum residual method.

The second equation of the Bergman iteration (7) is a least square problem. The solution is given by

$$(\lambda F_u^* F_u + \mu P^* P)s = \lambda F_u^* m + \mu P^*(A^T + Q) \qquad (12)$$

where $A^T = \alpha(P(s))$ and the superscript $*$ indicates the adjoint of the given operator. P^*P is a diagonal matrix and if every pixel appears with same frequency (Λ) in different patches, then $P^*P = \Lambda I$. $F_u^* F_u$ can be expressed as F^*U^*UF, where U^*U is also a diagonal matrix. Using above, Equation (12) can be rewritten as:

$$(\lambda F^*U^*UF + \mu\Lambda I F^* F)s = \lambda F_u^* m + \mu P^*(A^T) + Q),$$

which leads to direct analytical solution for s:

$$s = F^*(\lambda U^*U + \mu\Lambda I)^{-1}(\lambda U^* m + \mu F P^*(A^T + Q)). \qquad (13)$$

If the sampling strategy for the generation of patches is such that pixels don't appears with same frequency in different patches, then $(\lambda F_u^* F_u + \mu P^* P)$ cannot be diagonalized and Equation 7 needs to be solved using conjugate gradient descent algorithm. The overall algorithm is given in Algorithm 1.

A. IMPLEMENTATION

The algorithm was implemented in Matlab on a Ubuntu workstation with Intel core i7-6700K processor and 16GB RAM. The weight matrix W contains values to 25 nearest neighbors. VLFeat package [38], which implements a randomized

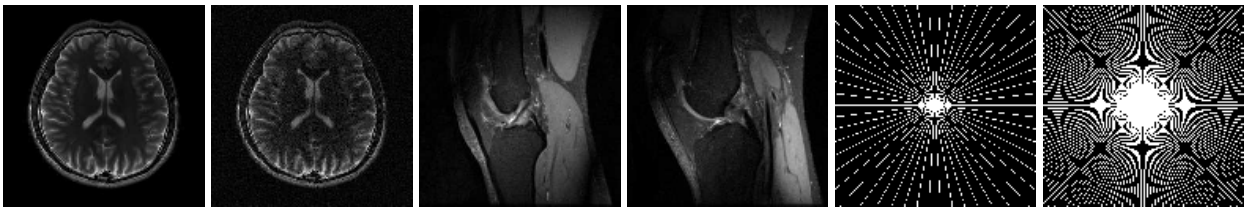

FIGURE 2. Sample images from the datasets. [First two]: Sample images from IXI dataset [40] [Middle two]: Sample images from the Knee dataset [41] [Last two]: Sampling radial masks used in the experiment corresponding to 10% and 30% sampling rates.

Algorithm 1 Proposed Compressed Sensing MRI Reconstruction Algorithm

Input : Initial guess of the MR image s^o, $Q^o = 0$
Output: Restored MR image s

while $||s^{k+1} - s^k||/||s^k|| > tol$ **do**
  Compute the $N \times N$ weight matrix W from $P(s^k)$ with $W_{ij} = \exp(\frac{-\|x_i - x_j\|^2}{\sigma^2})$, $x_i, x_j \in P(s^k)$ and $N = |P(s)|$;
  Compute the matrix $L = D - W$, where D is diagonal matrix with $D_i = \sum_{i=1}^{N} W_{ij}$;
  Solve the linear system $(L + \mu W)U = \mu WV$, where $V = (P(s^k) - Q^k)^T$;
  Update the image s^{k+1} using Equation (13) or Equation 14;
  $Q^{k+1} = Q^k + A^T - P(s^{k+1})$;
end

and approximate k-d forest [39], is used to search the nearest neighbors. This enabled fast nearest neighbor queries in high dimensional data points. The linear system in Equation (11) is asymmetric and is solved using Matlab implementation of generalized minimum residual method (GMRES). On average the algorithm took about 12 seconds/image to converge. The convergence condition is $||s^{k+1} - s^k||/||s^k|| < tol$.

If we assume that the k-space measurements are obtained noise free, i.e $m = F_u s$, then the solution to (7) can be obtained by the following equation,

$$s = F^*(\frac{1}{\Lambda}\hat{U}^*\hat{U}FP^*(A^T + Q) + U^*m), \tag{14}$$

where $\hat{U}$ is the binary inversion of the undersampling mask U.

IV. RESULTS

We evaluated the performance of our algorithm on two publicly available datasets of MR images (1) IXI database (the brain dataset) [40] and (2) Knees dataset [41]. We randomly selected 100 MR images from both the datasets for evaluation. The evaluations are carried out at sampling rates of 10% and 30% corresponding to 10× and 5× acceleration rates. Radial trajectories are used to sample the k-space. The radial trajectories are less sensitive to motion and therefore are preferred choice [42], [43]. Figure 2 shows some sample images from the two datasets and the radial sampling masks used in the experiment.

It is important to note that our experimental datasets are real-valued MR images and the K-space data is generated by taking the Fourier transform of the images. Experiment on complex-valued data is performed in Section V-B. The reconstruction error is gauged using three image quality metrics: normalized root-mean-square error (NRMS), structural similarity index measure (SSIM) and peak signal–to-noise ratio (PSNR). NRMSE is defined as:

$$\text{NRMS}(s) = \frac{\|s - \hat{s}\|}{\|\hat{s}\|} \tag{15}$$

where s and $\hat{s}$ are the reconstructed and the fully sampled MR images. SSIM is a perceptual metric that quantifies image quality degradation with reference to the original image. The PSNR is defined as

$$\text{PSNR}(s) = 10\,log_{10}\frac{\text{peakval}^2}{\text{MSE}(s, \hat{s})}, \tag{16}$$

where peakval is the maximum value of the signal, which in our case is 1. MSE$(s, \hat{s})$ is the mean-squared-error between the reconstructed and the fully sampled image. Lower values of NRMS and higher values of SSIM and PSNR indicate good reconstruction quality. Matlab functions were used to compute the three quality metrics with default parameters. The proposed method is compared against shift-invariant discrete wavelet transform based conventional CS-MRI method (SIDWT) [44], a dictionary learning-based method (DLMRI) [13] and a graph-based redundant wavelet transform method (GBRWT) [22]. Both DLMRI and GBRWT use overlapping images patches to sparsely represent the MR images. The default parameters for these methods are used in the image reconstruction.

Figure 3 shows the PSNR, SSIM and NRMS error graphs of the proposed and the comparison methods on 100 randomly chosen MR images from IXI brain dataset. Figure 5 shows a representative reconstruction of one MR image from the dataset at 10% and 30% sampling rate along with the error map of the zoomed in portion of the image. Similarly, Figure 4 shows the error graphs for the knee dataset and a representative reconstruction is shown in Figure 6. Overall, the proposed algorithm was able to reconstruct MR images with better PSNR, SSIM and NRMS than the

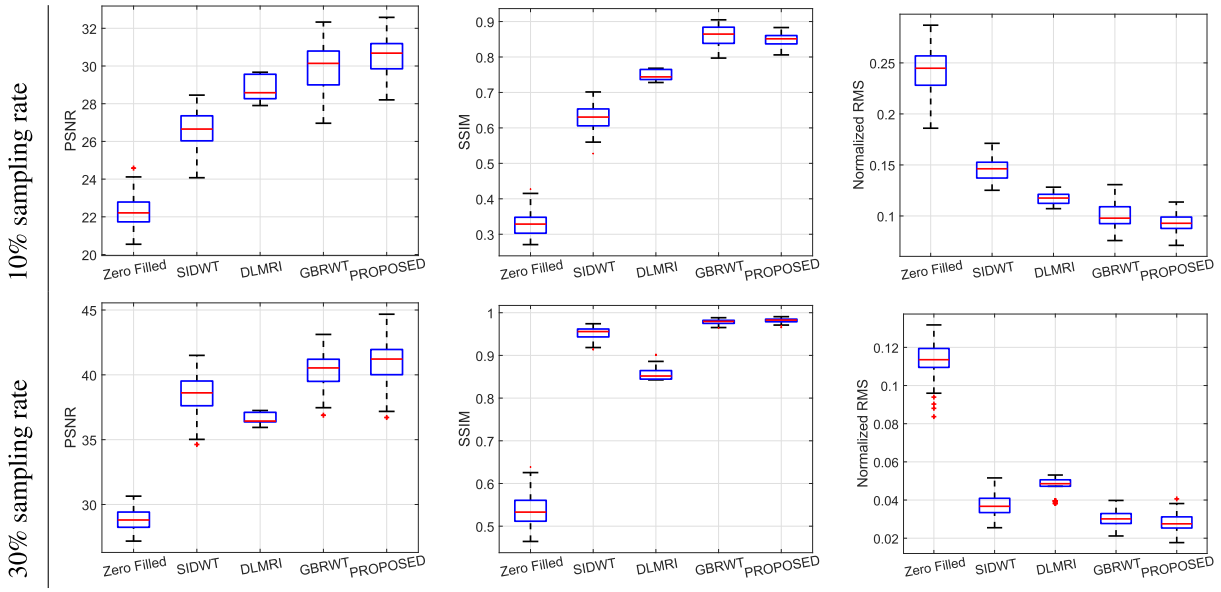

FIGURE 3. Evaluation on IXI Brain dataset [40].

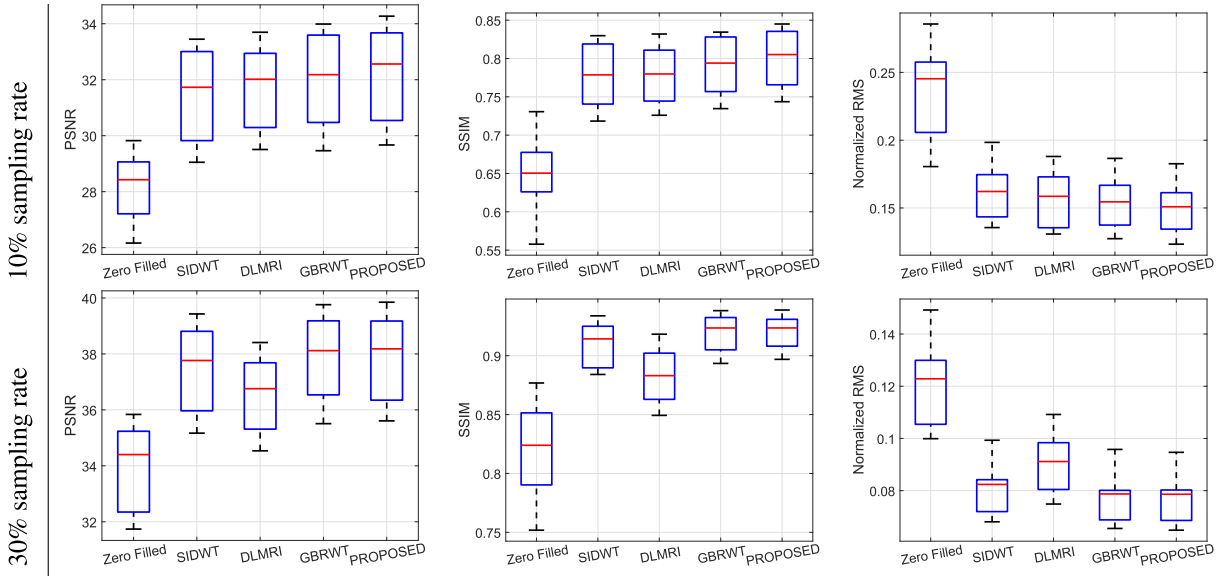

FIGURE 4. Evaluation on Knee dataset [41].

comparison methods. Only at 10% sampling rate, the SSIM of the proposed method on the IXI Brain dataset is slightly worse than the GBRWT method. But even in this case, the PSNR and NRMS are better than GBRWT.

The parameter values of the proposed algorithm are adjusted by first running the algorithm on few examples not present in the evaluation set with various parameter settings. The parameters giving the best reconstruction are then chosen. For IXI brain dataset, the $\mu = 1$, patches of block size 8×8 are used, with the stride of 1×1. The weight matrix is truncated to the 25 nearest neighbors. During the parameter adjustment phase, we noticed that for a highly undersampled reconstruction, a relatively higher σ value is required for the Gaussian weight function. We think that this allows for the neighboring patches to have a greater effect on the reconstruction of the patches. Therefore, σ is set to 0.3 and 0.1 for the sampling rates of 10% and 30%. For the Knee dataset, $\mu = 1$, patches of block size 24×24 are used, with the stride of 2×2. The σ is set to 0.6 and 0.3 for the sampling rates of 10% and 30%. These parameter values are then kept fixed for the whole dataset. The trade-off between fitting the observations and reducing the model complexity is handled by the parameter λ. For both datasets in this section, however, we assume that the k-space measurements m are noise free,

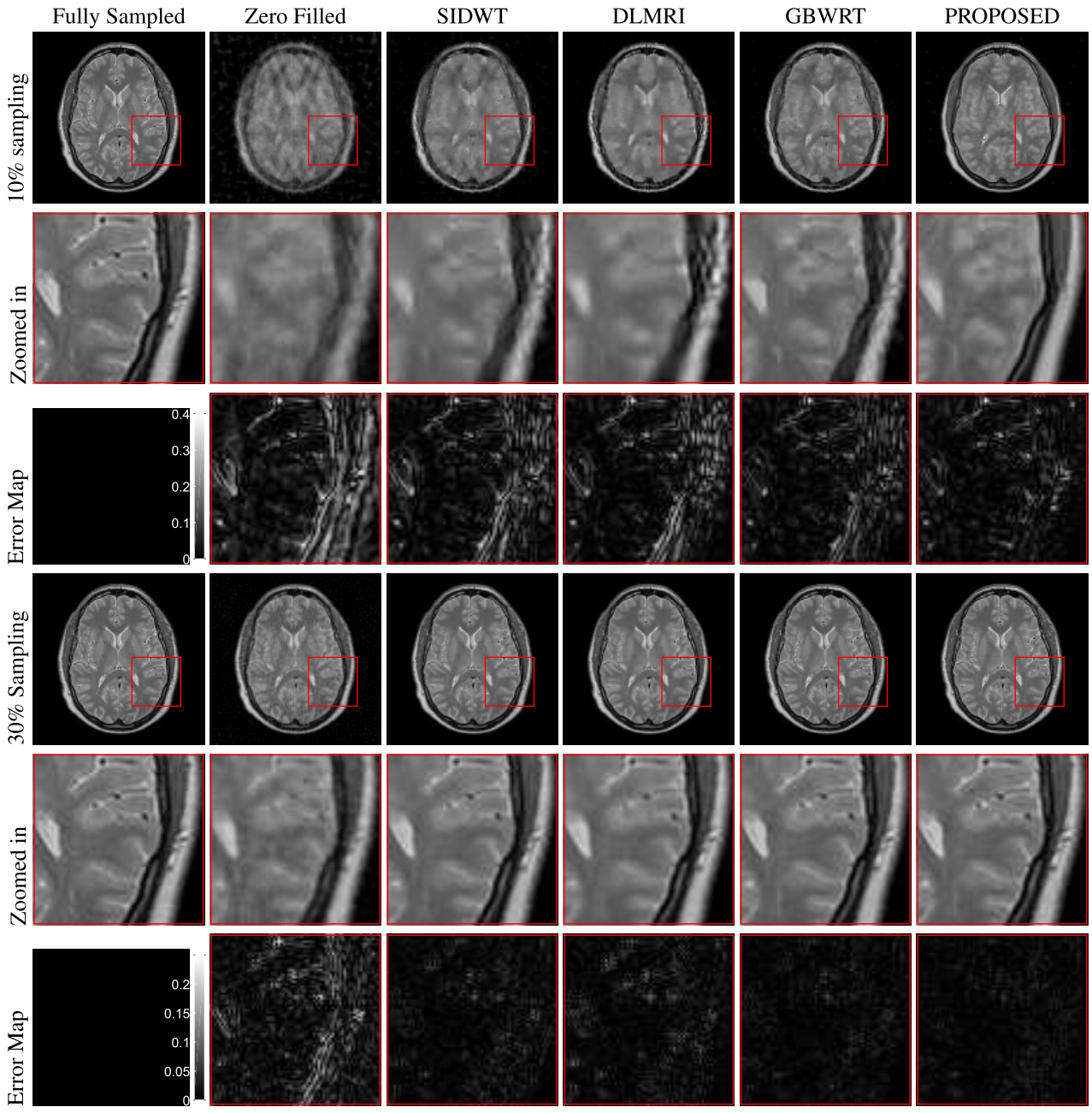

FIGURE 5. Visual image quality comparison on the IXI brain dataset at a sampling rate of 10% and 30%. The red box is zoomed-in in the subsequent row along with the error map compared to full reconstruction.

hence Equation (14) is used to update the current estimate of image (line no 5 of Algorithm 7). Note, that (14) does not include the parameter λ, as only the unobserved part of k-space is updated.

We used the output of SIDWT as initial guess s^0 in Algorithm 7. We noted that for the sampling rate of 10%, using either SIDWT or zero-filled reconstruction as s^0 gave same performances. However, for 30% sampling rate, the reconstruction was better with SIDWT as s^0 than zero-filled reconstruction. It should be mentioned that the comparison method GBRWT also uses SIDWT as initial guess. In Section V, we evaluate the effect of the initial image on the reconstruction of the proposed method. At 30% sampling rate, the weight matrix computation (Line 2 of Algorithm 7) can be moved outside the while loop, i.e weight matrix W is computed once and then kept fixed. This did not compromise the accuracy but reduced the computational time of the algorithm. On average, the algorithm took 20 seconds/image to converge on IXI brain dataset and 4 seconds on Knee dataset. On knee dataset, the algorithm required fewer iterations to converge to the solution. This may be due to the bigger patch block size.

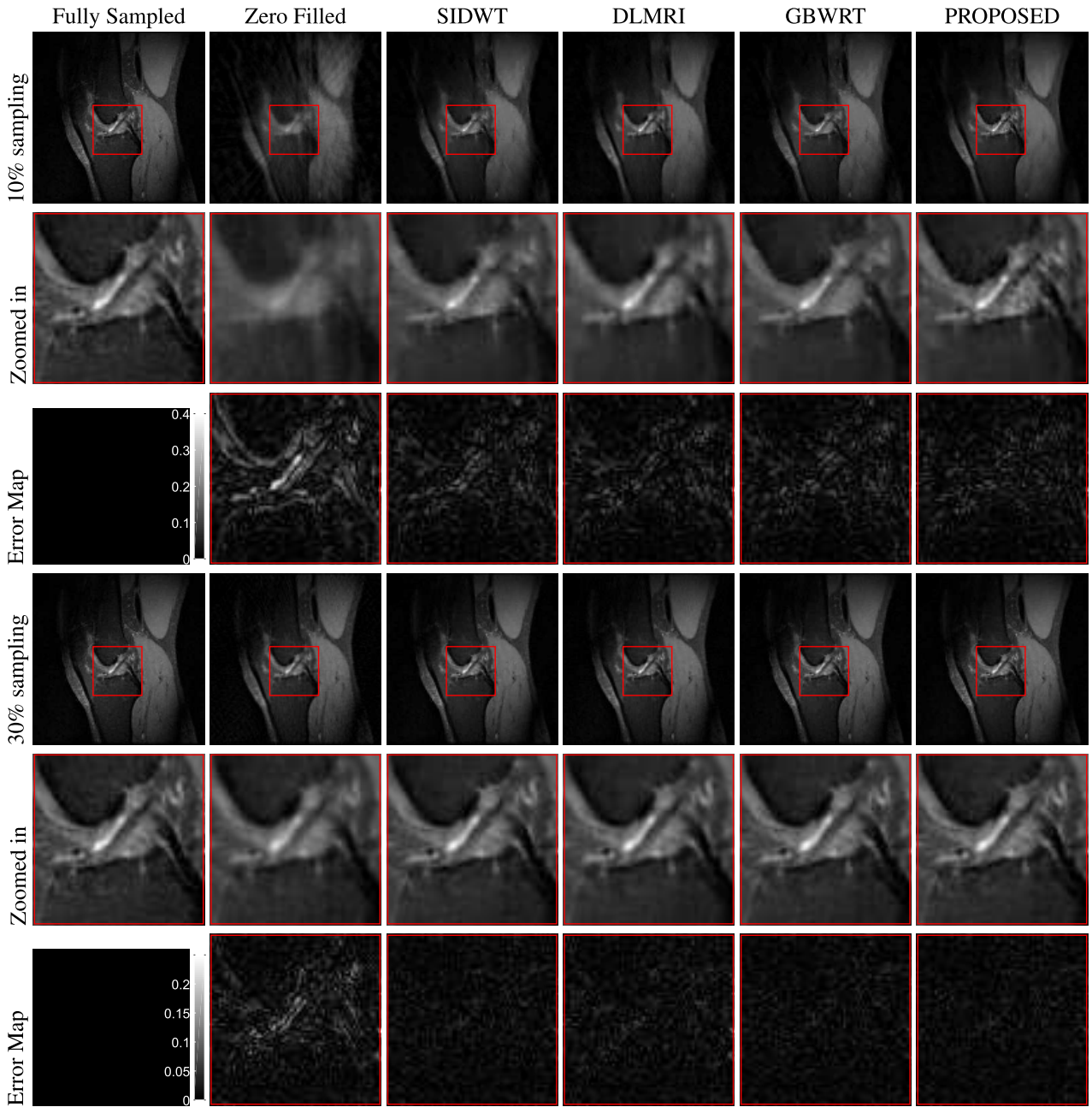

FIGURE 6. Visual image quality comparison on the Knee dataset at a sampling rate of 10% and 30%. The red box is zoomed-in in the subsequent row along with the error map compared to full reconstruction.

V. DISCUSSION

A. EFFECT OF INITIAL REFERENCE IMAGE

In the proposed algorithm the weight matrix W is computed using the patches from the current estimate of the MR image. If a good initial reference image is available then the weight matrix can be computed from the ground truth image once and not updated in each iteration. This significantly improves the image reconstruction quality and computation time. To evaluate the effect of the initial reference image, a fully sampled image and SIDWT-based image is used as reference image for both the proposed and GBRWT method [22]. For the proposed method, the weight matrix is computed once from the initial reference image and not updated again. Figure 7 shows the reconstruction of an MR image of 3DMR chest at 10% sampling rate using SIDWT-based and a fully sampled image as initial guess. The reconstruction is compared against GBRWT [22], where also a SIDWT and a fully sampled image is used as a reference image. The error maps are also shown with different colorbars for the two different initializations. Table 1 lists the values of the three quality metrics for both initializations, which shows that the proposed method outperforms GBRWT in both cases,

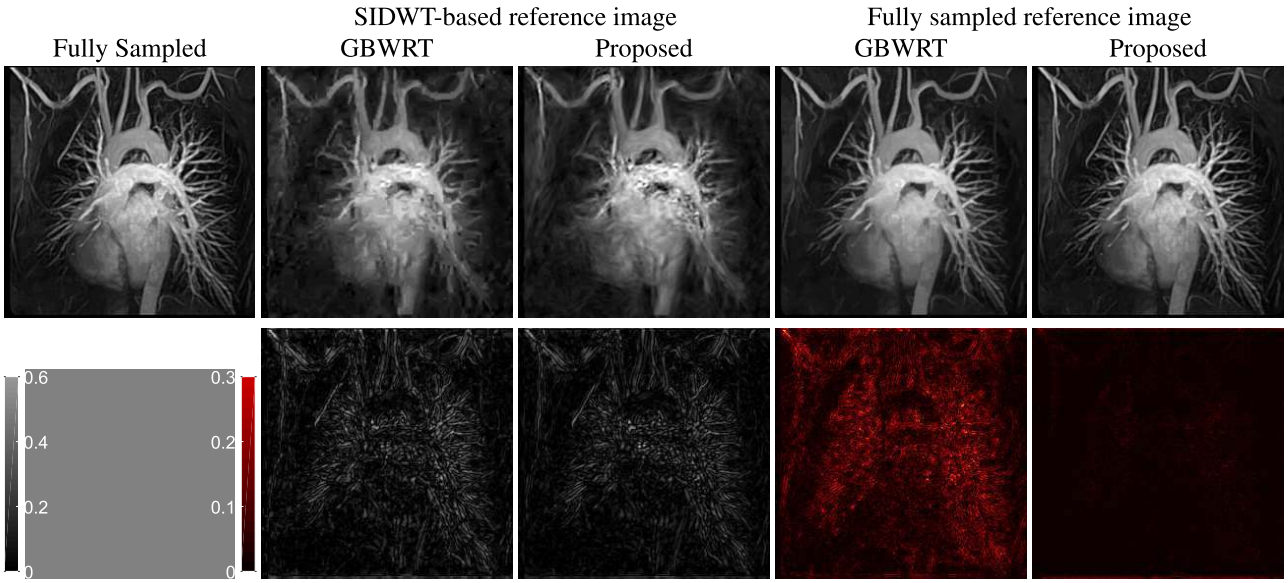

FIGURE 7. 3DMR Chest reconstruction at 10% undersampling rate using SIDWT and fully sampled image as reference. Bottom row shows the error map. The proposed method outperforms GBWRT in both cases, specially when better estimate for the initial image is available. See Table 1 for qualitative comparison. The experiment indicates that the proposed method has the greater ability to use the reference image.

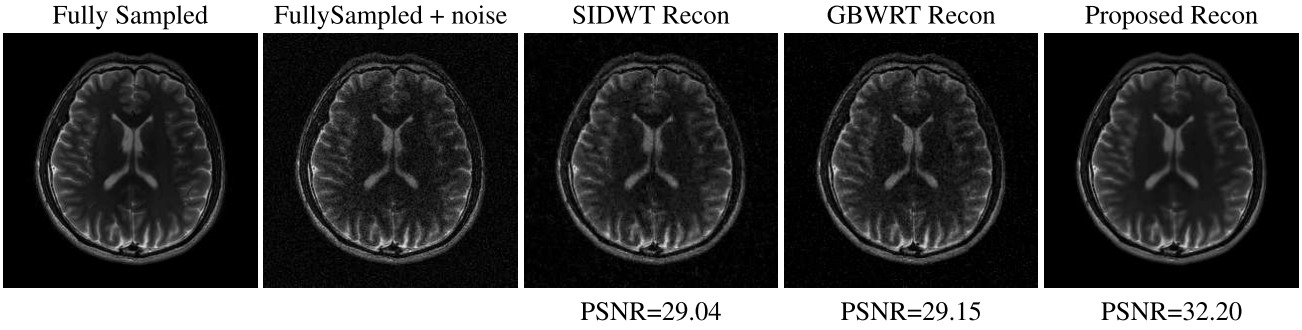

FIGURE 8. T2 Weighted Brain image reconstruction at 30% undersampling rate and Gaussian noise of $\sigma = .05$. The reconstruction of the proposed method successfully suppresses noise. See Table 2 for qualitative comparison with GBWRT at various noise levels.

TABLE 1. 3DMR Chest reconstruction at 10% undersampling rate using SIDWT and fully sampled image as reference.

Quality Metric	SIDWT		Fully Sampled	
	GBWRT	Proposed	GBWRT	Proposed
PSNR	23.16	**23.23**	31.22	**42.66**
SSIM	0.57	**0.58**	0.90	**0.99**
NRMS	0.22	**0.21**	0.08	**0.02**

more so when the better estimate of the MR image is available (PSNR of the proposed method is 42.66, while for GBWRT it is 31.22), indicating that the proposed method has greater ability to exploit the reference image.

B. EFFECT OF NOISE

To evaluate the effect of noise on the proposed method, we added Gaussian noise with std of $\sigma = \{.02, .05, .1\}$ on a fully sampled T2 weighted brain image. The reconstruction was carried out at 30% sampling rate. The block size for the generation of patches was set to 12×12 with stride 1×1. The weight matrix is truncated to 25 neighbors with $\sigma = .1$ and $\mu = 1$. Equation 13 is used to update the current estimate of image in line no 5 of Algorithm 7. λ is empirically determined to seek a balance between fitting the measurements and finding a reasonably low dimensional patch manifold. We have observed that $\lambda = 100$ gives good result in the presence of noise. The method is compared against GBWRT. For both methods, SIDWT-based reconstruction was used as s^0. Table 2 lists the values of the three quality metrics for three different noise levels, which shows that the proposed method outperform in all three quality metrics at various noise levels. Figure 8 shows the reconstruction at noise level $\sigma = .05$. The reconstruction shows the proposed method can suppress noise much better than GBWRT and SIDWT. The superiority of the proposed method in noisy compressive sensing in Table 2 comes from the low dimensional manifold model employed. As the noise level increases, the patch-manifold dimensions also increase.

TABLE 2. T2 weighted Brain image reconstruction at 30% undersampling rate at various noise levels.

	$\sigma = 0.02$		$\sigma = 0.05$		$\sigma = 0.1$	
Quality Metric	GBWRT	Proposed	GBWRT	Proposed	GBWRT	Proposed
PSNR	35.05	**35.31**	29.15	**32.20**	24.11	**27.02**
SSIM	0.8967	**0.95**	0.61	**0.90**	0.35	**0.54**
NRMS	0.12	**0.11**	0.24	**0.16**	0.43	**0.29**

By regularizing the manifold dimensions, the effect of noise on the reconstruction is reduced. Secondly, the parameters are kept fixed for the whole experiment, and not fine-tuned for various noise levels.

VI. CONCLUSION

The patch manifold of MR images exhibit low dimensional structure as illustrated in Figure 1. The low dimensionality of the patch manifold of the MRI images is used within the compressed sensing framework. The optimization problem is solved using split-Bregman iterations along with point integral method (PIM). The patches are generated such that each pixel appears with same frequency in different patches. With this setting, the current estimate of the image can be obtained using a direct analytical solution. The proposed method significantly enhances the anatomical structures of the reconstructed images. The reconstruction quality of the algorithm, gauged using the three quality metrics: peak signal-to-noise ratio (PSNR), structural similarity index measure (SSIM) and normalized root mean square error (NRMS), is better than the comparison methods. Future work will evaluate the utility of the proposed framework for dynamic MRI and 3-D MRI reconstruction.

REFERENCES

[1] B. Trémoulhéac, N. Dikaios, D. Atkinson, and S. R. Arridge, "Dynamic mr image reconstruction–separation from undersampled (k,t)-space via low-rank plus sparse prior," *IEEE Trans. Med. Imag.*, vol. 33, no. 8, pp. 1689–1701, Aug. 2014.
[2] D. J. Larkman and R. G. Nunes, "Parallel magnetic resonance imaging," *Phys. Med. Biol.*, vol. 52, no. 7, pp. R15–R55, 2007.
[3] D. L. Donoho, "Compressed sensing," *IEEE Trans. Inf. Theory*, vol. 52, no. 4, pp. 1289–1306, Apr. 2006.
[4] M. Lustig, D. Donoho, and J. M. Pauly, "Sparse MRI: The application of compressed sensing for rapid MR imaging," *Magn. Reson. Med.*, vol. 58, no. 6, pp. 1182–1195, 2007.
[5] M. Lustig, D. L. Donoho, J. M. Santos, and J. M. Pauly, "Compressed sensing MRI," *IEEE Signal Process. Mag.*, vol. 25, no. 2, pp. 72–82, Mar. 2008.
[6] L. Chaâri, J.-C. Pesquet, A. Benazza-Benyahia, and P. Ciuciu, "A wavelet-based regularized reconstruction algorithm for SENSE parallel MRI with applications to neuroimaging," *Med. Image Anal.*, vol. 15, no. 2, pp. 185–201, 2011.
[7] I. Khalidov, J. Fadili, F. Lazeyras, D. Van De Ville, and M. Unser, "Activelets: Wavelets for sparse representation of hemodynamic responses," *Signal Process.*, vol. 91, no. 12, pp. 2810–2821, Dec. 2011.
[8] Z.-P. Liang, "Spatiotemporal imagingwith partially separable functions," in *Proc. 4th IEEE Int. Symp. Biomed. Imag., Nano Macro*, Apr. 2007, pp. 988–991.
[9] J. P. Haldar and Z.-P. Liang, "Spatiotemporal imaging with partially separable functions: A matrix recovery approach," in *Proc. IEEE Int. Symp. Biomed. Imag., Nano Macro*, Apr. 2010, pp. 716–719.
[10] M. Lustig, J. M. Santos, D. L. Donoho, and J. M. Pauly, "K-T sparse: High frame-rate dynamic magnetic resonance imaging exploiting spatio-temporal sparsity ," U.S. Patent 7 602 183 B2, Oct. 13, 2009.
[11] S. G. Lingala, Y. Hu, E. DiBella, and M. Jacob, "Accelerated dynamic MRI exploiting sparsity and low-rank structure: k-t SLR," *IEEE Trans. Med. Imag.*, vol. 30, no. 5, pp. 1042–1054, May 2011.
[12] A. Majumdar and R. K. Ward, "An algorithm for sparse MRI reconstruction by schatten *p*-norm minimization," *Magn. Reson. Imaging*, vol. 29, no. 3, pp. 408–417, Apr. 2011.
[13] S. Ravishankar and Y. Bresler, "MR image reconstruction from highly undersampled k-space data by dictionary learning," *IEEE Trans. Med. Imag.*, vol. 30, no. 5, pp. 1028–1041, May 2011.
[14] Y. Huang, J. Paisley, Q. Lin, X. Ding, X. Fu, and X.-P. Zhang, "Bayesian nonparametric dictionary learning for compressed sensing MRI," *IEEE Trans. Image Process.*, vol. 23, no. 12, pp. 5007–5019, Dec. 2014.
[15] Y. Wang and L. Ying, "Compressed sensing dynamic cardiac cine MRI using learned spatiotemporal dictionary," *IEEE Trans. Biomed. Eng.*, vol. 61, no. 4, pp. 1109–1120, Apr. 2014.
[16] J. Caballero, A. N. Price, D. Rueckert, and J. V. Hajnal, "Dictionary learning and time sparsity for dynamic MR data reconstruction," *IEEE Trans. Med. Imag.*, vol. 33, no. 4, pp. 979–994, Apr. 2014.
[17] T. M. Quan and W.-K. Jeong, "Compressed sensing dynamic MRI reconstruction using GPU-accelerated 3D convolutional sparse coding," in *Proc. Int. Conf. Med. Image Comput. Comput.-Assist. Intervent.* Greece: Springer, 2016, pp. 484–492.
[18] G. Adluru, T. Tasdizen, M. C. Schabel, and E. V. R. DiBella, "Reconstruction of 3D dynamic contrast-enhanced magnetic resonance imaging using nonlocal means," *J. Magn. Reson. Imag.*, vol. 32, no. 5, pp. 1217–1227, Nov. 2010.
[19] D. Liang, H. Wang, Y. Chang, and L. Ying, "Sensitivity encoding reconstruction with nonlocal total variation regularization," *Magn. Reson. Med.*, vol. 65, no. 5, pp. 1384–1392, May 2011.
[20] X. Qu, Y. Hou, F. Lam, D. Guo, J. Zhong, and Z. Chen, "Magnetic resonance image reconstruction from undersampled measurements using a patch-based nonlocal operator," *Med. Image Anal.*, vol. 18, pp. 843–856, Aug. 2014.
[21] X. Qu, D. Guo, B. Ning, Y. Hou, Y. Lin, S. Cai, and Z. Chen, "Undersampled MRI reconstruction with patch-based directional wavelets," *Magn. Reson. Imag.*, vol. 30, no. 7, pp. 964–977, Sep. 2012.
[22] Z. Lai, X. Qu, Y. Liu, D. Guo, J. Ye, Z. Zhan, and Z. Chen, "Image reconstruction of compressed sensing MRI using graph-based redundant wavelet transform," *Med. Image Anal.*, vol. 27, pp. 93–104, Jan. 2016.
[23] M. Akçakaya, T. A. Basha, B. Goddu, L. A. Goepfert, K. V. Kissinger, V. Tarokh, W. J. Manning, and R. Nezafat, "Low-dimensional-structure self-learning and thresholding: Regularization beyond compressed sensing for MRI Reconstruction," *Magn. Reson. Med.*, vol. 66, no. 3, pp. 756–767, Sep. 2011.
[24] T. M. Quan, T. Nguyen-Duc, and W.-K. Jeong, "Compressed sensing MRI reconstruction using a generative adversarial network with a cyclic loss," *IEEE Trans. Med. Imag.*, vol. 37, no. 6, pp. 1488–1497, Jun. 2018.
[25] Q. Huang, D. Yang, P. Wu, H. Qu, J. Yi, and D. Metaxas, "MRI reconstruction via cascaded channel-wise attention network," Oct. 2018, *arXiv:1810.08229*. [Online]. Available: https://arxiv.org/abs/1810.08229
[26] S. Osher, Z. Shi, and W. Zhu, "Low dimensional manifold model for image processing," *SIAM J. Imag. Sci.*, vol. 10, no. 4, pp. 1669–1690, Oct. 2017.
[27] T. Goldstein and S. Osher, "The split Bregman method for L1-regularized problems," *SIAM J. Imag. Sci.*, vol. 2, no. 2, pp. 323–343, Apr. 2009.
[28] Z. Li, Z. Shi, and J. Sun, "Point integral method for solving Poisson-type equations on manifolds from point clouds with convergence guarantees," *Commun. Comput. Phys.*, vol. 22, no. 1, pp. 228–258, Jul. 2017.
[29] Z. Shi and J. Sun, "Convergence of the point integral method for Poisson equation on point cloud," Mar. 2014, *arXiv:1403.2141*. [Online]. Available: https://arxiv.org/abs/1403.2141
[30] W. Zhu, B. Wang, R. Barnard, C. D. Hauck, F. Jenko, and S. Osher, "Scientific data interpolation with low dimensional manifold model," *J. Comput. Phys.*, vol. 352, pp. 213–245, Jan. 2018.
[31] W. Zhu, Z. Shi, and S. Osher, "Scalable low dimensional manifold model in the reconstruction of noisy and incomplete hyperspectral images," May 2016, *arXiv:1605.05652*. [Online]. Available: https://arxiv.org/abs/1605.05652
[32] S. P. Ellis and M. McDermott, "Measuring the local dimension of point clouds," *Comput. Statist. Data Anal.*, vol. 17, pp. 317–326, Mar. 1994.
[33] M. Belkin and P. Niyogi, "Laplacian eigenmaps for dimensionality reduction and data representation," *Neural Comput.*, vol. 15, no. 6, pp. 1373–1396, Jun. 2003.

[34] M. Usman, G. Vaillant, D. Atkinson, T. Schaeffter, and C. Prieto, "Compressive manifold learning: Estimating one-dimensional respiratory motion directly from undersampled k-space data," *Magn. Reson. Med.*, vol. 72, no. 4, pp. 1130–1140, Oct. 2014.
[35] S. Poddar and M. Jacob, "Dynamic MRI using smoothness regularization on manifolds (SToRM)," *IEEE Trans. Med. Imag.*, vol. 35, no. 4, pp. 1106–1115, Apr. 2016.
[36] X. Chen, M. Usman, C. F. Baumgartner, D. R. Balfour, P. K. Marsden, A. J. Reader, C. Prieto, and A. P. King, "High-resolution self-gated dynamic abdominal MRI using manifold alignment," *IEEE Trans. Med. Imag.*, vol. 36, no. 4, pp. 960–971, Apr. 2017.
[37] S. T. Roweis and L. K. Saul, "Nonlinear dimensionality reduction by locally linear embedding," *Science*, vol. 290, no. 5500, pp. 2323–2326, Dec. 2000.
[38] A. Vedaldi and B. Fulkerson, "VlFeat: An open and portable library of computer vision algorithms," in *Proc. 18th ACM Int. Conf. Multimedia*, Oct. 2010, pp. 1469–1472.
[39] M. Muja and D. G. Lowe, "Fast approximate nearest neighbors with automatic algorithm configuration," in *Proc. VISAPP*, 2009, vol. 2, nos. 331–340, pp. 1–10.
[40] *IXI Dataset*. http://brain-development.org/ixi-dataset/
[41] K. Epperson, A. M. Sawyer, M. Lustig, M. Alley, M. Uecker, P. Virtue, P. Lai, and S. Vasanawala, "Creation of fully sampled MR data repository for compressed sensing of the knee," in *Proc. Meeting SMRT*, Salt Lake City, UT, USA, Apr. 2013.
[42] L. Feng, R. Grimm, K. T. Block, H. Chandarana, S. Kim, J. Xu, L. Axel, D. K. Sodickson, and R. Otazo, "Golden-angle radial sparse parallel MRI: Combination of compressed sensing, parallel imaging, and golden-angle radial sampling for fast and flexible dynamic volumetric MRI," *Magn. Reson. Med.*, vol. 72, no. 3, pp. 707–717, Sep. 2014.
[43] D. C. Peters, R. J. Lederman, A. J. Dick, V. K. Raman, M. A. Guttman, J. A. Derbyshire, and E. R. McVeigh, "Undersampled projection reconstruction for active catheter imaging with adaptable temporal resolution and catheter-only views," *Magn. Reson. Med.*, vol. 49, no. 2, pp. 216–222, Feb. 2003.
[44] C. A. Baker, K. King, D. Liang, and L. Ying, "Translational-invariant dictionaries for compressed sensing in magnetic resonance imaging," in *Proc. IEEE Int. Symp. Biomed. Imag., Nano Macro*, Mar./Apr. 2011, pp. 1602–1605.

SAIM ABDULLAH received the B.S. degree in computer science from FAST National University, Faisalabad, Pakistan. He is currently pursuing the master's degree with the School of Electrical Engineering and Computer Science (SEECS), National University of Sciences and Technology, Islamabad, Pakistan. His research interest includes artificial intelligence and its applications.

OMAR ARIF received the B.E. degree in software engineering from the National University of Sciences and Technology (NUST), Islamabad, Pakistan, and the M.S. and Ph.D. degrees in electrical and computer engineering from the Georgia Institute of Technology, Atlanta, USA. He is currently the Head of the Software Engineering Department, NUST. His current research interests include machine learning and computer vision.

M. BILAL ARIF received the M.B.B.S. degree from Quaid-i-Azam University, Islamabad, Pakistan, in 2001, and the Fellowship in internal medicine (FCPS Pakistan), in 2010. He is currently a Consultant in internal medicine with CMH Pano Aqil, Pakistan.

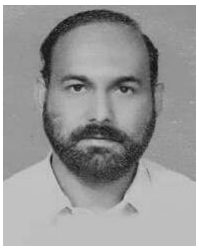

TAHIR MAHMOOD received the M.B.B.S. degree from Peshawar University, Pakistan, MCPS (medicine) CPSP, the master's degree in critical care medicine from Quaid-i-Azam University, Islamabad, the M.Phil. degree in microbiology from Hazara University, Mansehra. He is currently a Principal Medical Officer with Benazir Bhutto Shaheed Teaching Hospital.